

RSC Advances



This is an *Accepted Manuscript*, which has been through the Royal Society of Chemistry peer review process and has been accepted for publication.

Accepted Manuscripts are published online shortly after acceptance, before technical editing, formatting and proof reading. Using this free service, authors can make their results available to the community, in citable form, before we publish the edited article. This *Accepted Manuscript* will be replaced by the edited, formatted and paginated article as soon as this is available.

You can find more information about *Accepted Manuscripts* in the [Information for Authors](#).

Please note that technical editing may introduce minor changes to the text and/or graphics, which may alter content. The journal's standard [Terms & Conditions](#) and the [Ethical guidelines](#) still apply. In no event shall the Royal Society of Chemistry be held responsible for any errors or omissions in this *Accepted Manuscript* or any consequences arising from the use of any information it contains.

ARTICLE

Electronic structures of two types of TiO₂ electrodes: inverse opal and nanoparticulate cases

Cite this: DOI: 10.1039/x0xx00000x

Taro Toyoda,^{*a,d} Witoon Yindeesuk,^a Tsuyoshi Okuno,^a Masaya Akimoto,^a Keita Kamiyama,^b Shuzi Hayase,^{c,d} and Qing Shen^{*a,d}

We present a comparison between the electronic structures of inverse opal (IO) and nanoparticulate (NP)-TiO₂ electrodes. The electronic structure details were obtained from optical absorption, fluorescence, and valence band studies in order to clarify the nature of the higher photovoltaic performance observed in sensitized solar cells using IO-TiO₂ electrodes. We used photoacoustic (PA) and photoluminescence (PL) spectroscopy to characterize the optical absorption and fluorescence properties, respectively. Photoelectron yield (PY) spectroscopy was applied to characterize the position of the valence band maximum (VBM) of the IO- and NP-TiO₂ electrodes. The PA spectrum for IO-TiO₂ is different to that for NP-TiO₂, indicating differences in the exciton-phonon interactions and the density of states in the conduction band. PL measurements showed that the curvature of the valence band structure of IO-TiO₂ is different to that of NP-TiO₂. Also, PL measurements showed that the oxygen vacancy in IO-TiO₂ is different to that in NP-TiO₂. Moreover, PY measurements showed VBM in IO-TiO₂ to be at a higher position than that in NP-TiO₂, suggesting a correlation with the increased open circuit voltage (V_{oc}) in sensitized solar cells.

Received 00th January 2012,
Accepted 00th January 2012

DOI: 10.1039/x0xx00000x

www.rsc.org/

Introduction

Titanium dioxide (TiO₂) is an important oxide semiconductor, used in numerous technological applications such as photocatalysis and solar energy conversion.¹ Nanostructured TiO₂ is of tremendous importance for improving charge collection efficiency and photochemical activity. For the last two decades, much attention has been devoted to dye-sensitized solar cells (DSCs) made from nanostructured TiO₂ electrodes, firstly because of their high photovoltaic conversion efficiency, which exceeds 10%, and secondly, because the technology to manufacture them is low cost.^{1,2} In DSCs, the organic dye molecules, which act as photosensitizers, and nanostructured TiO₂, which is the recipient/electron transport layer for electrons injected from the optically excited sensitizer, improve the light harvesting efficiency. One promising approach in the development of third-generation solar cells is to exchange the

the organic dye by semiconductor quantum dots (QD-sensitized solar cells: QDSCs). Firstly, semiconductor QDs can be utilized as photosensitizers, since their bandgap (or HOMO-LUMO gap) can be tuned by controlling the size of the dots so that the absorption spectrum matches the spectral distribution of sunlight.³ Secondly, they possess high extinction coefficients and large intrinsic dipole moments, leading to rapid charge separation.⁴ Thirdly, semiconductor QDs have the potential for multiple exciton generation (MEG), which can potentially increase the photovoltaic conversion efficiency up to 44%.⁵⁻⁸ For the last decade much attention has been devoted to QDSCs with nanostructured TiO₂ electrodes.⁹⁻²³

One of the main factors determining the photovoltaic performance of sensitized solar cells is the morphology of the TiO₂ electrodes, which has an effect on the sensitizer assembly and, consequently, the photovoltaic conversion efficiency. The morphology of the TiO₂ electrodes, including the crystal structure and surface orientation, is important, because this has a strong influence on the photovoltaic properties.^{19-21,24-26} In sensitized solar cells, the nanostructured TiO₂ electrodes have a large surface area which increases the loading of the sensitizer thus enhancing light harvesting. On the other hand, the recombination process is proportional to the electrode surface area. The recombination process has a significant effect on the open-circuit voltage, V_{oc} . A balance between recombination and light harvesting is needed to maximize solar cell performance.^{27,28} Another factor is the transport of photogenerated electrons through the nanostructured TiO₂ electrode network. The results suggest that the photovoltaic

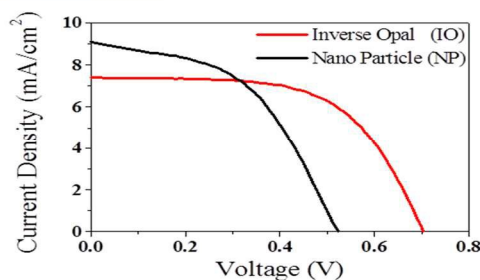
^aDepartment of Engineering Science, The University of Electro-Communications, 1-5-1 Chofugaoka, Chofu, Tokyo 182-8585, Japan. E-mail: toyoda@pc.uec.ac.jp, shen@pc.uec.ac.jp; Fax: +81-42-443-5501; Tel. +81-42-443-5464

^bBunkoukeiki Co. Ltd, 4-8 Takakura, Hachioji, Tokyo 192-0033, Japan

^cGraduate School of Life Science and Systems Engineering, Kyushu Institute of Technology, 2-4 Hibikino, Wakamatsu-ku, Kitakyushu, Fukuoka 808-0196, Japan

^dCore Research for Evolutional Science and Technology (CREST), Japan science and Technology Agency (JST), 4-1-8 Honcho, Kawaguchi, Saitama 332-0012, Japan

conversion efficiency can be further enhanced by having a more efficient electron transport path through the TiO₂ electrodes. To accomplish higher photovoltaic conversion efficiency, recent research has focused on using electrodes with an ordered structure rather than a randomly packed nanoparticulate TiO₂ (NP-TiO₂) structure.^{19,29,30} The relatively low photovoltaic conversion efficiency obtained with sensitized solar cells compared to that with conventional Si solar cells and the theoretical value of the Shockley-Queisser detailed balance limit (~ 31%)³¹ are ascribed to the poor penetration of the sensitizers and redox couples into thick TiO₂ electrodes. To address the penetration of both the sensitizers and the redox couples, an approach has been proposed using mesoporous inverse opal (IO)-TiO₂ produced from self-organizing systems.^{32,33} IO-TiO₂ electrodes have a honeycomb structure with large interconnected pores that lead to better infiltration despite the smaller surface area than NP-electrodes.¹⁹ In addition, depending on the filling fraction of the TiO₂, a photonic bandgap is formed in the photonic crystal,³⁴⁻³⁷ which gives the possibility of enhancing the light harvesting efficiency. Photonic crystals have unique structural properties and optical characteristics, which have been utilized not only in solar cells^{11,12,20,38-45} but also in photocatalysis.⁴⁶⁻⁴⁸ In DSC and QDSC applications, there are several reports claiming that V_{oc} can be increased by about 30% by using IO-TiO₂ electrodes.^{11,12,19,41-45} In order to study the unique properties of IO structure in sensitized solar cell applications, the typical photovoltaic performance of CdSe QD-sensitized IO-TiO₂ and NP-TiO₂ solar cells were compared, which have been characterized in our laboratory, as shown in Fig. 1. The thickness of both TiO₂ films was similar (~ 3 μm). The short circuit current, J_{sc} , of solar cells with IO-TiO₂ electrodes (7.4 mA/cm²) is a little smaller than those with NP-TiO₂ electrodes (9.1 mA/cm²) in spite of the smaller specific surface area of IO-TiO₂ electrode than that of NP-TiO₂ electrode. A higher V_{oc} is observed with IO-TiO₂ electrodes compared to conventional NP-TiO₂ electrode, resulting a higher photovoltaic conversion efficiency (3.2 %) than that of NP-TiO₂ case (2.2 %), although the amount of CdSe QDs in the IO-TiO₂ case is smaller than the NP-TiO₂ due to the difference specific surface area.¹⁹ The higher V_{oc} observed in the IO-TiO₂ case is a superior characteristics compared to NO-TiO₂ ones. However, the key



Electrode	J_{sc} (mA/cm ²)	V_{oc} (V)	FF	η (%)
Inverse Opal	7.4	0.69	0.60	3.2
Nanocrystal	9.1	0.52	0.49	2.2

Fig. 1 Current density-voltage characteristics in CdSe-sensitized IO-TiO₂ and NP-TiO₂ solar cells with the same thickness. Parameters in the photovoltaic solar cells are listed in the table.

factors that determine the enhancement of V_{oc} still remain unclear. It appears that fundamental studies are needed to shed light on the underlying physics and chemistry governing the enhancement of the photovoltaic conversion efficiency. Nevertheless, a detailed analysis of the effects of the nanostructured morphology on the electronic structure of TiO₂ has not yet been studied, neither experimentally nor theoretically. In this work, we compare the electronic structures of IO-TiO₂ and NP-TiO₂, the details for which were obtained from optical absorption, fluorescence, and valence band studies. A fundamental understanding of the comparison between the electronic structures including the surface chemistries of IO-TiO₂ and NP-TiO₂ is lacking, and this deficiency needs to be addressed to determine the factors leading to the enhancement of V_{oc} . In general, it is necessary to develop suitable combinations of QDs and nanostructured TiO₂ electrodes with different morphologies to enhance photovoltaic conversion efficiencies of QDSCs.

Initially, information regarding the optical absorption properties of IO- and NP-TiO₂ was needed to investigate the absorption edge and sub bandgap absorption with the aim of carrying out studies on photosensitization by QDs. The samples used in this study optically scatter light and we applied photoacoustic (PA) spectroscopy to measure the optical absorption characteristics. PA spectroscopy is a branch of photothermal spectroscopy in which heating the sample causes the selective absorption of the optical energy. The PA technique detects the acoustic energy produced by heat generated through nonradiative processes in materials.⁴⁹ The PA signal is less sensitive to light scattering effects than conventional transmission signals.^{21,25,26,50-52} The PA sensitivity is higher for weak absorption than that of conventional transmission techniques due to the induced thermal energy. Hence, the technique is useful not only for optical absorption edge characterization but also for sub bandgap characterization. For characterizing the exciton and defect states in IO- and NP-TiO₂, photoluminescence (PL) spectroscopy can be applied although the results in the literature on the PL characteristics of TiO₂ are rarely consistent to explain this clearly.⁵³ Moreover, PL spectroscopy has been employed as an important tool in studies of the electronic structures and optical properties of many different nanostructured materials,^{54,55} and therefore supplementary information on the differences between the electronic structures of IO- and NP-TiO₂ can be obtained. In addition to the characterization by PA and PL spectroscopies, photoelectron yield (PY) spectroscopy^{56,57} is applied to characterize the position of the valence band maximum (VBM) which is correlated with the photovoltaic properties, especially V_{oc} , since V_{oc} is related to the difference between the Fermi level of the electrode material and the redox potential in the electrolyte. As PY spectroscopy does not need complex energy corrections in the data analysis, it is expected to have an advantage in analyzing dielectric materials. By utilizing this characteristic of PY spectroscopy, direct observations of the positions of VBM in IO- and NP-TiO₂ can be realized with which the effect of morphological differences can be evaluated without the need for special techniques. .

Experimental

Materials and chemicals

The preparation method for IO-TiO₂ electrodes has been reported in a previous study.⁴⁰ Fluorine-doped tin oxide (FTO) conducting glass (10 Ω/sq) was ultrasonically cleaned in

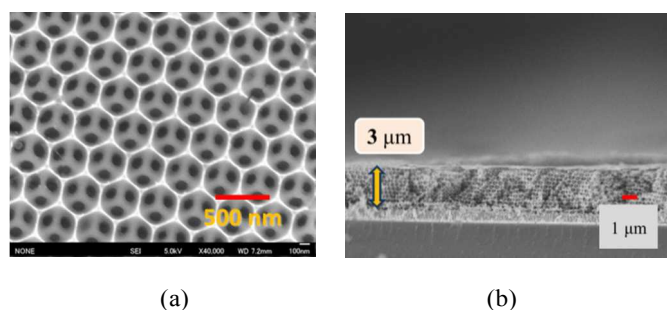


Fig. 2 Scanning electron microscopy (SEM) images of IO-TiO₂ ((a) top view, (b) side view).

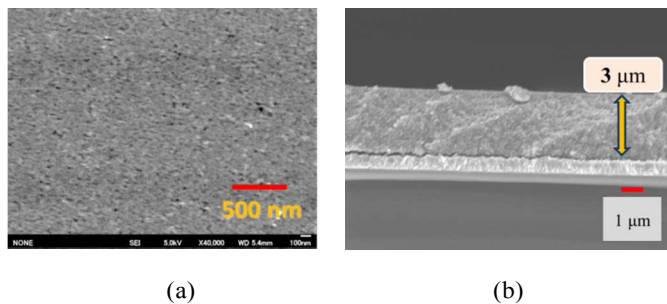


Fig. 3 Scanning electron microscopy (SEM) images of NP-TiO₂ ((a) top view, (b) side view).

detergent, KOH, distilled water, and methanol. A uniform polystyrene (PS) latex suspension (474 nm in diameter) was agitated by ultrasound for 30 min to split the aggregated particles. The fabricated opal samples were prepared by dipping the FTO substrate vertically in a 0.1 wt.% monodispersed PS suspension and evaporating the solvent in an oven at 40°C slowly leaving behind a colloidal PS film on the substrate as a template.³² Then the TiO₂ was brought into the voids in the template by the following method. A 10 μl drop of 2% TiCl₄ in methanol was added via a micropipette onto the PS colloidal crystal surface. After hydrolysis for 30 min, the sample was subsequently heated to 80°C in air. This process was repeated three times to ensure the filling of all the voids. Finally, the sample was heated at 450°C for 1 h in air with a ramp rate of 0.5°C/min to calcinate the template and anneal the TiO₂. After calcination of the latex template, a honeycomb structure appeared with an ordered hexagonal pattern of spherical pores that connected each sphere to its nearest neighbors. Typical scanning electron microscopy (SEM) images of IO-TiO₂ are shown in Fig. 2 ((a) top view; (b) side view). The diameter or center to center distance of the pores, referred to as the periodic lattice constant of IO-TiO₂, was determined to be ~380 nm (Fig. 2 (a)) which shows the amount of shrinkage suffered by the 474 nm diameter PS latex particles. This structure consists of several layers connected to each other (Fig. 2 (a) and (b)). The TiO₂ thickness was measured as 3 μm using a contact profilometer (DEKTAC, ULVAC Co., Ltd, Japan). The reflection spectrum of IO-TiO₂ using 474 nm PS latex particles had a peak at 710 nm, indicating that the IO-TiO₂ has a photonic crystal character. This peak value is in good agreement with the Bragg reflection in a photonic crystal.⁴⁰ In order to ascertain the influence the electrode morphology has, conventional NP-TiO₂ electrodes were prepared by a combination of 15 nm NP-TiO₂ (Super Titania, Showa Denko, Co., Ltd, Japan) and polyethylene glycol (molecular weight: 500,000) in distilled water. In our experiments, we showed the

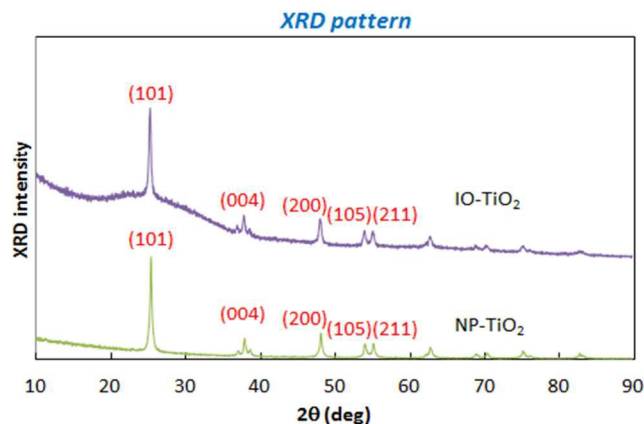


Fig. 4 X-ray diffraction (XRD) patterns of IO-TiO₂ and NP-TiO₂.

optimal conditions for QDSCs was to use 15 nm NP-TiO₂. The prepared pastes were applied onto FTO substrates using the doctor blade method, followed by sintering at 450°C for 30 min in air. Typical SEM images of NP-TiO₂ are shown in Fig. 3 ((a) top view; (b) side view), which shows a randomly packed NP-TiO₂ structure both in the top and side views. The thickness was measured as 3 μm. The x-ray diffraction (XRD) patterns of IO- and NP-TiO₂ are shown in Fig. 4. The characteristic diffraction peaks of both IO- and NP-TiO₂ at 2θ values of 25.3°, 37.9°, 48.1°, 54.0°, 55.2°, and 62.8° can be assigned to the (101), (004), (200), (105), (211), and (204) faces of anatase TiO₂, respectively.⁴⁸ IO- and NP-TiO₂ have similar XRD patterns, suggesting that the three-dimensional periodic structure (IO-TiO₂) does not have an impact on the TiO₂ crystalline phase. The crystallite domain sizes of IO- and NP-TiO₂ were characterized by applying Scherrer equation in (101) XRD peak. The width of the half-maximum of the XRD peaks in (101) is identical with each other (~0.015 rad). Hence, the crystal domain size of IO-TiO₂ is same as that of NP-TiO₂ (~11 nm), also indicating that the three-dimensional periodic structure (IO-TiO₂) does not have an impact on the TiO₂ crystalline phase. Preliminary AFM observations show that IO-TiO₂ wall consists of TiO₂ nanoparticles with several tens order and size of NP-TiO₂ is also close to several tens order consistent with the use of 15 nm nanoparticles (aggregation). The Brunauer-Emmett-Teller (BET) method was applied to characterize the specific surface areas of IO- and NP-TiO₂. The specific surface areas of IO- and NP-TiO₂ are 35 m²/g and 80 m²/g, respectively, indicating that the former is smaller than the latter (one half of the latter).

PA spectroscopic characterization

The optical absorption properties of IO- and NP-TiO₂ were investigated using a single beam PA spectrometer. A typical gas-microphone technique was applied in the PA measurements.⁴⁹ The sample was placed inside a closed cell (PA cell) containing air. The PA cell was composed of an aluminum cylinder with a small channel at the periphery in which a microphone was inserted. The light source was a 300 W xenon short arc lamp. Monochromatic light through a monochromator was modulated at frequencies of 33, 133, and 233 Hz to investigate the effect of saturation.⁴⁹ Modulated monochromatic light was focused onto the sample surface located inside the sealed PA cell. Light absorbed by the sample was changed into periodic heating by a nonradiative process,

which results in a pressure variation due to the air inside the cell (acoustic wave). The PA signal was monitored by first passing the microphone output through a preamplifier and then a lock-in amplifier synchronized with the modulation frequency. The data were averaged to improve the signal-to-noise ratio (S/N). The spectra were taken at room temperature in the wavelength range of 300 – 830 nm. The optical absorption length for wavelengths from 350 to 830 nm is longer than the thermal diffusion length and the thickness of sample, indicating that the PA signal intensity is proportional to the optical absorption coefficient.⁴⁹ In this case (optically transparent and thermally thin solid conditions), the PA intensity (P) is given by the relationship,

$$P = A\beta l, \quad (1)$$

where A is a constant, β is the optical absorption coefficient, and l is the thickness of the sample.⁴⁹ The spectra were calibrated by the PA measurement from a carbon black sheet that was proportional to the incident light intensity due to the fact that the optical absorption length is shorter than the thermal diffusion length in the wavelength range concerned.⁴⁹ A UV cut filter was used for the measurements in the wavelength range of 600 – 830 nm to avoid mixing with second harmonic light. The experimental conditions for the measurements were fixed as far as possible to compare each of the PA spectra directly.

PL spectroscopic characterization

The PL spectra were measured using a He-Cd laser (325 nm, 20 mW) as an excitation light source at room temperature.⁵⁸ When the semiconductor surface is illuminated by light with sufficient energy above the bandgap, photons are absorbed strongly. Electrons are excited from the VB to the conduction band (CB), leaving a hole in the VB. The electron and hole can recombine producing PL through several deexcitation processes. The PL was measured with a single monochromator and CCD detection. The spectra were taken at room temperature in the wavelength range of 350 – 900 nm.

PY spectroscopic characterization

The PY spectra were collected using an ionized energy measurement system (BIP-KV201, Bunkoukeiki, Co., Ltd., Japan). A negative bias was applied to a base plate behind the sample against the grounded anode for the PY measurements. The number of photoelectrons was obtained by measuring the current needed to compensate for the photoexcited holes at the sample with an ammeter. In the PY measurements, the photoemission yield Y was measured as a function of photon energy ($h\nu$) and the value of the ionization potential (I) can be determined from the onset of the PY spectrum. The PY spectrum around the photoelectric threshold I is usually expressed by the following relation

$$Y = B (h\nu - I)^n, \quad (2)$$

where B is a constant and n is a parameter which mainly depends

on the shape of the density of electronic states at the upper edge of the occupied states and the transmission probability of electrons across the surface.⁵⁶ The square-root law ($n = 2$) and cube root law ($n = 3$) are often used for fitting the PY spectra of metals and organic materials, respectively.^{56,59} In this work, we employed $n = 3$ based on the theoretical analysis.^{56,59} The plot of the values of $Y^{1/3}$ as a function of $h\nu$ obtained here show a fairly linear relationship at the onset. The value of I was determined by extrapolating the linear part of $Y^{1/3}$ to the baseline. An energy scan of the incident photons was performed while increasing the photon energy of the UV light (4 ~ 9.5 eV). The UV light was focused on the sample over an area of $1 \times 3 \text{ mm}^2$. All measurements were performed in a vacuum chamber ($\sim 4 \times 10^{-3}$ Pa) at room temperature.

Results and discussion

PA characteristics of IO- and NP-TiO₂

The shape of the PA spectrum is independent of the modulation frequency concerned, indicating that the PA spectra reflect the optical absorption characteristics (the optical absorption length is longer than the thermal diffusion length). The influence of the absorption of the FTO (SnO₂, bandgap: 3.6 eV) substrate is low, since the thickness of this is $\sim 500 \text{ nm}$ thicker than that of TiO₂ ($\sim 3 \mu\text{m}$). According to equation (1) the PA intensity is proportional to the thickness of the sample. The spectra are normalized at a photon energy of 3.7 eV. To clarify the subtle distinction between the spectra for IO- and NP-TiO₂, we show

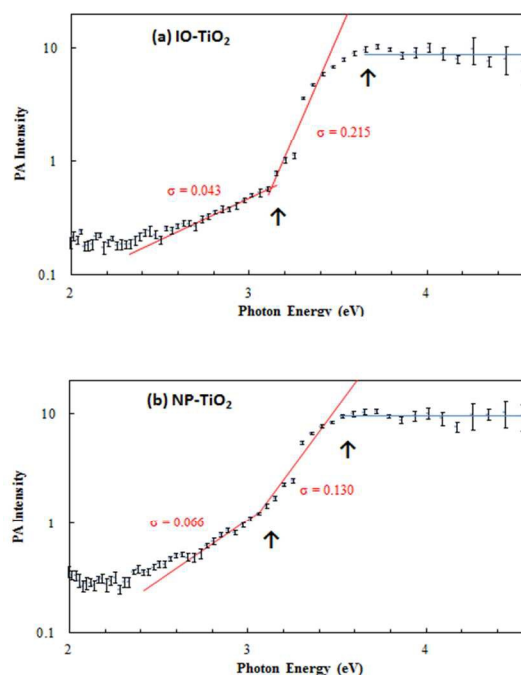


Fig. 5 Photoacoustic (PA) spectra of (a) IO-TiO₂ and (b) NP-TiO₂ (semi-logarithmic scale).

the logarithmic PA intensities ((a) IO-TiO₂ and (b) NP-TiO₂) at a modulation frequency of 133 Hz as a function of photon energy in Fig. 5. In the case of the semiconductors, both for direct and indirect transitions, the band edge as measured by the position of the knee (an inflection point) in the logarithmic PA spectrum agrees very well with the values recorded in the literature.⁶⁰ Also, the low energy tail of the absorption edge depends exponentially on the photon energy (Urbach rule).⁶¹ Figure 5 shows that the logarithmic PA intensity varies linearly as a function of photon energy in two regions (2.8 – 3.2 eV and 3.2 – 3.7 eV), indicating the possibility of two optical absorption processes.⁶⁰ These two steps variations are inherent in TiO₂ and are not due to instrumental reasons since other semiconductor samples, such as CdS and CdSe (direct transition case), show one step variation in PA intensity in our measurements similar to the reference.⁶⁰ The positions of the knees are shown as arrows (↑) in Fig. 5. The position in the lower energy region (2.8 – 3.2 eV) for the IO-TiO₂ spectrum agrees with that in NP-TiO₂ (~ 3.2 eV), possibly indicating the first bandgap energy of anatase TiO₂. A short modified energy level diagram of anatase TiO₂ is depicted in Fig. 6, where Γ denotes the center of the Brillouin zone (BZ) and X the edge of BZ.⁶²⁻⁶⁴ The VB of anatase TiO₂ is composed principally of oxygen 2p orbitals, with the corresponding wave functions considerably localized on the O²⁻ latt ice sites. The CB consists mostly of Ti⁴⁺ excited states.⁶³ The arrows in Fig. 6 indicate direct allowed (↑: blue) and indirect allowed (↑: red) transitions, respectively. The level X_{2a} is positioned at zero energy for simplicity.⁶²⁻⁶⁴ The positions of the first arrow in the lower energy region in both IO- and NP-TiO₂ (2.8 – 3.2 eV, ~ 3.2 eV) in Fig. 6 are ascribed to the indirect band transition, $\Gamma_3 \rightarrow X_{1b}$, according to the references.⁶²⁻⁶⁴ The position of the second arrow in the higher energy region (3.2 – 3.7 eV) in IO-TiO₂ (~ 3.63 eV) is a little higher than that of NP-TiO₂ (~ 3.52 eV). The possible reason for the difference in the position of the arrows between IO- and NP-TiO₂ is the difference in thermal properties between IO- and NP-TiO₂.⁴⁹ However, the positions of the arrows in the IO- and NP-TiO₂ spectra are independent of the modulation frequency, indicating that there is little possibility of a difference in thermal properties. Within the experimental accuracy, those positions are ascribed to the direct band transitions, X_{2b} → X_{1b} for IO-TiO₂ (theoretical value: 3.59 eV)

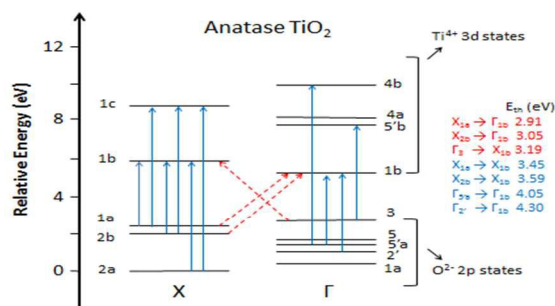


Fig. 6 Short energy diagram of anatase TiO₂.⁶³⁻⁶⁴

and X_{1a} → X_{1b} (theoretical value: 3.45 eV) for NP-TiO₂, respectively.⁶²⁻⁶⁴ Two steps variations similar to our results with indirect and direct transitions in absorption spectra were measured in Ge (indirect transition: 0.62 eV; direct transition: 0.81 eV) and Si (indirect transition: 1.06 eV; direct transition: 2.5 eV).⁶⁵ Thus, indirect and direct band transitions in TiO₂ can be observed separately by applying PA spectroscopy, owing to the lower sensitivity to light scattering effect.

Preliminary, we have prepared IO-TiO₂ by applying the different TiO₂ precursor with mixtures of absolute ethanol, hydrochloric acid, tetrabutyl titanate, and deionized water.⁶⁶ The PA spectra of IO-TiO₂ with different precursor and different periodic constant (200 – 600 nm) showed the same spectra which were identical with Fig. 5, indicating the possibility that the PA spectrum in IO-TiO₂ is independent of preparation method and periodic constant.

Studies of the exponential tail (Urbach rule) give basic information about the exciton-phonon interaction, band structure, and disordered states.⁶⁷⁻⁷² Here, we analyze and discuss the Urbach tails in the PA spectra of IO- and NP-TiO₂ using phenomenological models that have been extensively used for semiconductors.⁶¹ The dependence of the PA intensity of the exponential tail on the photon energy at a given temperature (T) is given by the empirical relationship

$$P = P_0 \exp\left\{\frac{\sigma(h\nu - h\nu_0)}{kT}\right\}, \quad (3)$$

where P is the PA intensity as a function of photon energy ($h\nu$), h is Planck's constant, ν is frequency ($h\nu$ corresponds to photon energy), k is the Boltzmann constant, and P_0 , σ , ν_0 are fitting parameters.⁶¹ Here, σ is a characteristic of the logarithmic slope (exponential tail) below the fundamental absorption edge and is called the steepness parameter. Also, the Urbach energy is defined as $E_U = kT/\sigma$, which indicates the width of the exponential tail in the PA spectra. We assume that the value of σ (or E_U) in the lower energy region (2.8 – 3.2 eV) is a reflection of the exciton-photon interaction in the oxide semiconductor crystal.⁷³ In this model, the interaction of excitons with a phonon causes the Urbach tail. The effects of disorders and impurities are taken into account in the exciton-phonon interaction. When the exciton-phonon interaction increases, the optical absorption below the band edge energy increases. Hence, the value of σ decreases or E_U increases. Toyozawa and co-workers, ascribed the Urbach tail to the influence of phonon fields on the center-of-mass motion of excitons, i.e., the momentary self-trapping of excitons.^{73,74} Smaller σ (or larger E_U) corresponds to a broader Urbach tail, and hence to larger exciton-phonon interactions, which has been generally accepted on the basis of various kinds of observation. The steepness parameter is proportional to the inverse of the exciton-phonon coupling constant.⁷⁵ In the lower energy region (2.8 – 3.2 eV), the value of σ in IO-TiO₂ (0.043 or $E_U = 600$ meV) is smaller than that in NP-TiO₂ (0.066 or $E_U = 390$ meV) (Fig. 5), indicating that the exciton-phonon interaction

in IO-TiO₂ is higher than that in NP-TiO₂ including the effect from the oxygen vacancies which is discussed later. In the higher energy region (3.2 – 3.7 eV), we assume that the value of σ (or E_U) is a reflection of the band structure, especially the density of states, in the oxide semiconductor crystal with the hypothesis that the optical transition probability in IO-TiO₂ is the same as that in NP-TiO₂. In the higher energy region (3.2 – 3.7 eV), the value of σ in IO-TiO₂ (0.215 or $E_U = 120$ meV) is higher than that in NP-TiO₂ (0.130 or $E_U = 200$ meV), indicating a higher density of states in the conduction band in IO-TiO₂ than that in NP-TiO₂. The possibility of the higher density of states in the conduction band of IO-TiO₂ is the overlap of wavefunctions due to a long-range electronic connectivity.

The absence of visible absorption peaks in the PA measurements below a photon energy of 3.0 eV in Fig. 5 does not indicate that oxygen vacancies are absent in IO- and NP-TiO₂. As IO- and NP-TiO₂ are luminescent materials (the details are discussed later), when an optically excited energy level decays via luminescence partially (radiative transition), a lower PA signal is produced due to the fact that PA signal is proportional to nonradiative transition probabilities.⁶⁰ The PA intensities of IO-TiO₂ below a photon energy of 3.0 eV are one half smaller than those of NP-TiO₂, indicating the possibility that the radiative transition probabilities by defect states in IO-TiO₂ is higher than that of NP-TiO₂ in the photon energy region. In the future, the comparison of the PL excitation spectra and PA spectra of IO- and NP-TiO₂ are needed to reveal the relaxation processes of photoexcited electrons.

PL characteristics of IO- and NP-TiO₂

In order to confirm the presence of defects in IO- and NP-TiO₂, PL measurements were carried out on those samples. The PL method is a sensitive technique for finding the presence of defect related excitation peaks. The excitation wavelength used was 325 nm, corresponding to a photon energy of 3.82 eV, higher than the indirect and direct bandgaps of the investigated TiO₂. At first step, time resolved PL spectra were attempted over 1 ms time domain both in IO- and NP-TiO₂ to investigate the nature of luminescence. As a result of the measurements, no luminescence signals were detected over 1 ms time domain, indicating the possibility that the luminescence is not phosphorescence but fluorescence. Also, there is a possibility that the IO- and NP-TiO₂ show fluorescence, since IO- and NP-TiO₂ indicate anatase structures in which lifetime is several tens of ns according to the references.^{76,77} The PL spectra of IO- and NP-TiO₂ are shown in Fig. 7. The PL spectra have broad bands in the visible range. The PL spectrum for IO-TiO₂ exhibits three distinct luminescence peaks at ~3.2 eV (↑: black), ~3.1 eV (↑: red), and ~2.2 eV with a broad band from 1.8 to 2.5 eV (↔). The PL spectrum for NP-TiO₂ also exhibits three distinct peaks at ~3.2 eV (↑: black), ~2.9 eV (↑: red), and ~2.6 eV (↑: blue). The peaks at ~3.2 eV in IO- and NP-TiO₂ are attributed to phonon assisted indirect transition from X_{1b} → Γ_3 in the Brillouin zone.⁶²⁻⁶⁴ IO- and NP-TiO₂ exhibit intense emission peaks at ~3.1 eV and ~2.9 eV, respectively, which are assigned to self-trapped excitons (STE) localized on TiO₆ octahedra.⁷⁸⁻⁸⁰ The difference between the

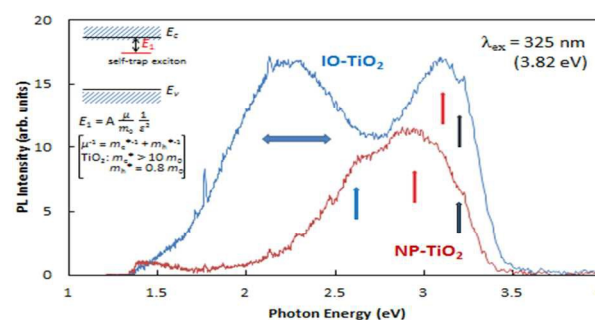


Fig. 7 Photoluminescence (PL) spectra of IO- and NP-TiO₂.

bottom of the conduction band and the self-trapped exciton state (E_1) in IO-TiO₂ is smaller (~0.1 eV) than that in NP-TiO₂ (~0.3 eV). The value of E_1 is given by the relationship (hydrogen model)

$$E_1 = A \frac{\mu}{m_0} \frac{1}{\epsilon^2}, \quad (4)$$

where A is a constant, m_0 is the electron rest mass, ϵ is the dielectric constant of the semiconductor, and μ is the reduced mass.⁸¹ The reduced mass is defined as $\mu^{-1} = m_e^{*-1} + m_h^{*-1}$, where m_e^* and m_h^* are the electron and hole effective masses, respectively. In general, the values for the effective electron and hole masses of TiO₂ are $m_e^* \geq 10 m_0$ and $m_h^* \approx 0.8 m_0$, respectively.⁸² Therefore, m_h^* is predominant in determining the value of E_1 ($E_1 \sim m_h^*$). The PL measurements show that the reduced mass μ of IO-TiO₂ is smaller than that of NP-TiO₂, suggesting that m_h^* of IO-TiO₂ is smaller than that of NP-TiO₂. The effective mass is defined as the inverse of the curvature of the E - k curve (band structure). So, there is a difference in the valence band structure between IO- and NP-TiO₂, indicating that the curvature of the E - k curve on the valence band in IO-TiO₂ is larger than that in NP-TiO₂. The larger curvature of the E - k curve on the valence band of IO-TiO₂ is the overlap of wavefunctions due to a long-range electronic connectivity.

The PL bands on the lower photon energy side of anatase TiO₂ nanoparticles have been attributed to oxygen vacancies at the surface.⁶³ In the lower photon energy region, IO- and NP-TiO₂ exhibit oxygen vacancy related emission peaks at ~2.2 eV and ~2.6 eV, respectively, in agreement with the reported values.⁶³ We suppose that there are two possibilities to identify those two emission peaks. One possibility is as follows. Since TiO₂ is semi-covalent material^{83,84} (ionicity: ~50%), the two emission peaks are ascribed to F^+ (~2.2 eV) and F (~2.6 eV) centers, respectively, referred to the references.^{79,80,85} The F^+ and F centers are oxygen-ion vacancies, the former with a trapped single electron and the latter occupied by two electrons. In IO-TiO₂, the oxygen vacancies of the F^+ centers might be larger than those in NP-TiO₂ and there is a possibility that those of the F centers are smaller than NP-TiO₂, indicating a difference in the vacancy structure between IO- and NP-TiO₂. Another possibility of the two peaks is the difference of the stoichiometry in IO- and

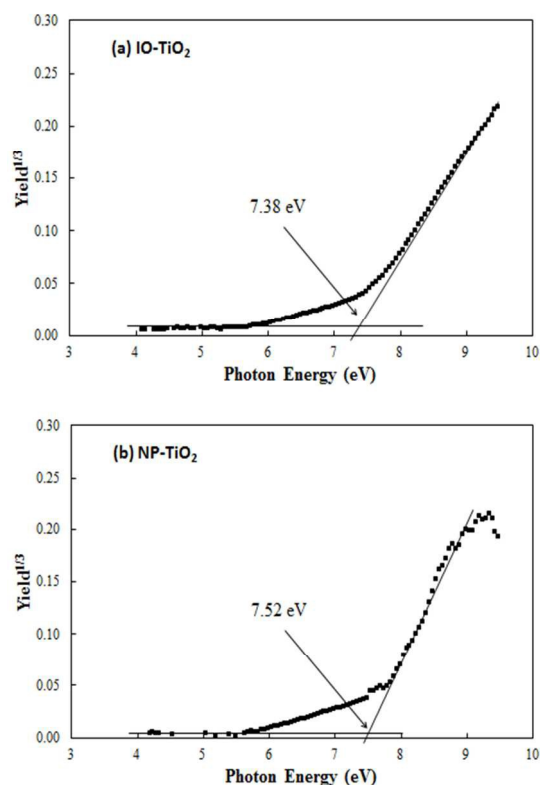


Fig. 8 Photoelectron yield (PY) spectra of (a) IO-TiO₂ and (b) NP-TiO₂.

NP-TiO₂. Preliminary, we have measured the PL of IO-TiO₂ which are prepared by different method⁶⁶ as mentioned in the PA spectroscopic characterization. The PL spectra showed the similar spectra as in Fig. 7. In this respect, it is important to investigate the differences in the concentration of oxygen vacancies. Detailed experiments on the concentration and electronic structure of oxygen vacancies are desirable for future investigations to clarify the nature of the difference of the vacancy states in IO- and NP-TiO₂. Also, the comparison of the PA and PL excitation spectra between IO- and NP-TiO₂ are needed to reveal the nature of electronic structure and oxygen vacancy states in the future.

PY characteristics of IO- and NP-TiO₂

Figure 8 shows the PY spectra ((a) IO-TiO₂ and (b) NP-TiO₂) as a function of photon energy. As the PY signal intensity has a good S/N ratio, an error bar is included for each point. The positions of VBM of IO- and NP-TiO₂ can be regarded as the ionization potential on the basis of the intersection of the tangent to the spectra with the baseline. We applied straight lines above a photon energy of 8.3 eV (linear region). The positions of VBM measured for IO- and NP-TiO₂ were -7.38 ± 0.05 and -7.52 ± 0.05 eV, respectively. Figure 9 shows the relative band edge positions of VBM and CBM for IO- and NP-TiO₂ together with those for the (111), (101), and (001) surfaces of anatase TiO₂ single crystal. The band gap value of 3.2 eV from the results in

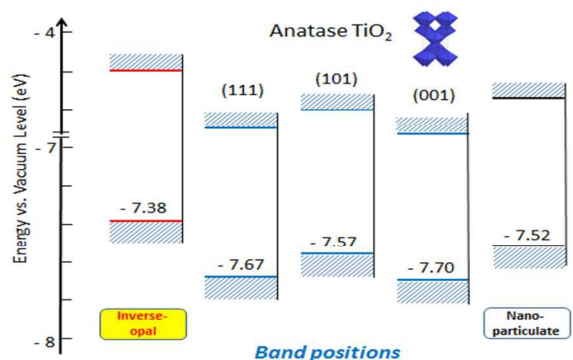


Fig. 9 Relative band edge positions of the valence band maximum (VBM), the conduction band minimum (CBM) together with those on the (111), (101), and (001) surfaces of anatase TiO₂ single crystals.

Fig. 5 is used for both IO- and NP-TiO₂ to determine the positions of the conduction minimum (CBM). The positions of VBM for (111), (101), and (001) surfaces of anatase TiO₂ single crystals are -7.67 ± 0.05 , -7.57 ± 0.05 , and -7.70 ± 0.05 eV, respectively, showing slight difference between each surfaces. The observed positions of VBM in anatase single crystals are different from those observed in rutile TiO₂ single crystals, indicating differences in the electronic structure and surface states.²⁶ The positions of VBM and CBM in IO-TiO₂ are higher than those in NP-TiO₂. Also, the positions of VBM and CBM in IO-TiO₂ are higher than those for the (111), (101), and (001) surfaces of anatase TiO₂ single crystals. Anatase TiO₂ single crystal has a few fundamental low-index facet systems. Typical anatase TiO₂ single crystals, including natural grown crystals, consist mostly of (101) surfaces ($\sim 80\%$) due to the much greater stability of this surface than the other surfaces due to its lower surface energy. Therefore, the characteristics of TiO₂ nanoparticles have mostly been attributed to the (101) surface.⁸⁶ The position of VBM in NP-TiO₂ (-7.52 eV) is close to that of the (101) surface of anatase TiO₂ (-7.57 eV), indicating that NP-TiO₂ consists mostly of (101) surfaces. Therefore, the higher position of VBM of IO-TiO₂ than that of NP-TiO₂ cannot be explained by a special surface orientation effect. The ionization potential of the surface of a semiconductor material is defined as the difference in the potential energy of an electron between the vacuum level and the position of VBM. The vacuum level is the energy of an electron at rest at a point sufficiently far outside the surface so that the electrostatic image force on the electron is neglected. The orientation of the exposed crystal surface affects the value of the ionization potential because the strength of the electric double layer at the surface depends on the concentration of positive ion cores on the surface. The double layer exists because the surface ions are in an asymmetrical environment, with vacuum on one side and the substrate on the other. Therefore, the PY measurements show that the formation of the double layer in IO-TiO₂ is different from that in NP-TiO₂. Recently, a method to produce a low-work function electrode by surface modification was realized.⁸⁷ The surface of IO-TiO₂ has a

larger distribution of oxygen vacancies assumed to F^+ centers with trapped single electrons than NP-TiO₂. As a result, the electric double layer in IO-TiO₂ is different from that in NP-TiO₂, indicating that IO-TiO₂ is polarized with a more positive dipole moment towards the vacuum level⁸⁸ than that of NP-TiO₂. Hence, the ionization potential in IO-TiO₂ is lower than that in NP-TiO₂, and a higher position of VBM in IO-TiO₂ (lower-ionization potential) than that in NP-TiO₂ (higher-ionization potential) can be achieved, suggesting a correlation with the increased V_{oc} in sensitized solar cells. Moreover, Hanmin et al. proposed the influencing factors for V_{oc} of sensitized solar cells.⁸⁹ The main influencing factors are the electron back-propagation constant K_{et} and the semiconductor light-free concentration n_0 . Our preliminary V_{oc} decay measurement of IO-TiO₂ shows longer decay time (~ 8s) than that of NP-TiO₂ (~ 1s), indicating that the K_{et} of IO-TiO₂ is lower than that of NP-TiO₂. Lower K_{et} corresponds to the increase of V_{oc} .⁸⁹ Also, n_0 of IO-TiO₂ is higher than that of NP-TiO₂, since the density of states of IO-TiO₂ in conduction band is higher than that of NP-TiO₂. Higher n_0 corresponds to the increase of V_{oc} .⁸⁹ These facts suggest the possibility of the increase of V_{oc} in IO-TiO₂.

Conclusions

One of the main factors determining the photovoltaic performance in sensitized solar cells is the morphology of the TiO₂ electrode. The assembly of the sensitizers depends on the morphology and using a suitable morphology can lead to improvements in the photovoltaic conversion efficiency. A higher open circuit voltage, V_{oc} , was observed with IO-TiO₂ electrodes compared to conventional NP-TiO₂ electrodes. However, the key factors that determine the enhancement of V_{oc} still remain unclear. It appears that fundamental studies are needed to shed light on the underlying physics and chemistry governing the enhancement of V_{oc} . Optical absorption measurements by the PA method showed that indirect and direct transitions can be observed in IO- and NP-TiO₂. The indirect bandgaps of IO- and NP-TiO₂ are similar to each other (~ 3.2 eV), and the direct bandgaps of them are ~ 3.6 eV and ~ 3.5 eV, respectively, indicating differences in the electronic structure. The density of states in the conduction band of IO-TiO₂ is larger than that of NP-TiO₂. Analysis of the Urbach tail shows there is a higher exciton-phonon interaction in IO-TiO₂ than in NP-TiO₂. Indirect PL and exciton PL can be observed. Also, PL due to oxygen vacancies was observed. The PL spectra suggest differences in the valence band structure between IO- and NP-TiO₂, indicating that the curvature in the valence band of IO-TiO₂ ($E-k$ curve) is larger than that of NP-TiO₂. The position of VBM for IO-TiO₂ is higher than that for NP-TiO₂, indicating that the surface of IO-TiO₂ is polarized with a more positive dipole moment towards the vacuum level than that of NP-TiO₂. Hence, the formation of a double layer in the former is different from that in the latter due to the differences in the formation of oxygen vacancies, suggesting a correlation with the increased V_{oc} in sensitized solar cells.

Acknowledgements

Part of this work was supported by Core Research for Evolutional Science and Technology (CREST), Japan Science Technology Agency (JST). Also, it was supported by JSPS Kakenhi Grant Number 26390016. We also thank T. Amano and Y. Takeshita of Bunkoukeiki Co., Ltd. for cooperation with the photoelectron yield spectroscopy measurements. We wish to acknowledge D. Tai, Y. Kuwano, and M. Hironaka for helping the sample preparation.

Notes and references

- 1 X. Chen and S. S. Mao, *Chem. Rev.*, 2007, **107**, 2891-2959.
- 2 M. A. Green, K. Emery, K. Hishikawa, W. Warta and E. D. Dunlop, *Prog. Photovoltaic. Res. Appl.*, 2012, **20**, 12-20.
- 3 W. W. Yu, L. Qu, W. Guo and X. Pen, *Chem. Mater.*, 2003, **15**, 2854-2860.
- 4 E. F. Underwood, T. Kippeny and S. J. Rosental, *Eur. Phys. J. D*, 2001, **16**, 241-244.
- 5 A. J. Nozik, *Physica E*, 2002, **14**, 115-120.
- 6 R. D. Schaller, M. Sykora, J. M. Pietryga and V.I. Klimov, *Nano Lett.*, 2006, **6**, 424-429.
- 7 V. I. Klimov, *J. Phys. Chem. B*, 2006, **110**, 16827-16845.
- 8 M. T. Trinh, A. J. Houtepen, J. M. Schins, T. Hanrath, J. Piris, W. Knulst, A. P. L. M. Goossens and L. D. A. Siebbeles, *Nano Lett.*, 2008, **8**, 1713-1718.
- 9 Q. Shen, D. Arae and T. Toyoda, *J. Photochem. Photobiol. A*, 2004, **164**, 75-80.
- 10 O. Niitsoo, S. K. Sarkar, P. Pejoux, R. Rühle, D. Cahen and G. Hodes, *J. Photochem. Photobiol. A*, 2006, **182**, 306-311.
- 11 L. J. Diguna, Q. Shen, A. Sato, K. Katayama, T. Sawada and T. Toyoda, *Mater. Sci. Eng. C*, 2007, **27**, 1514-1520.
- 12 L. J. Diguna, Q. Shen, J. Kobayashi and T. Toyoda, *Appl. Phys. Lett.*, 2007, **91**, 023116.
- 13 A. Kongkanand, K. Tvrđy, K. Takechi, M. Kuno and P. V. Kamat, *J. Am. Chem. Soc.*, 2008, **130**, 4007-4015.
- 14 I. Mora-Seró, S. Giménez, F. Fabregat-Santiago, R. Gómez, Q. Shen, T. Toyoda and J. Bisquert, *Acc. Chem. Res.*, 2009, **42**, 1848-1857.
- 15 I. Mora-Seró and J. Bisquert, *J. Phys. Chem. Lett.*, 2010, **1**, 3046-3052.
- 16 H. Tada, M. Fujishima and H. Kobayashi, *Chem. Soc. Rev.*, 2011, **40**, 4232-4243.
- 17 K. Tvrđy, P. A. Frantsukov and P. V. Kamat, *Proc. Nat. Acad. Sci.*, 2011, **108**, 29-34.
- 18 S. Emin, S. P. Singh, L. Han, N. Satoh and A. Islam, *Sol. Energy*, 2011, **85**, 1264-1282.
- 19 T. Toyoda and Q. Shen, *J. Phys. Chem. Lett.*, 2012, **3**, 1885-1893.
- 20 W. Yindeesuk, Q. Shen, S. Hayase and T. Toyoda, *AIP Adv.*, 2013, **3**, 102115.
- 21 T. Toyoda, Y. Onishi, K. Katayama, T. Sawada, S. Hayase and Q. Shen, *J. Mater. Sci. Eng. A*, 2013, **3**, 601-608.

- 22 M. A. Becker, J. G. Radich, B. A. Bunker and P. V. Kamat, *J. Phys. Chem. Lett.*, 2014, **5**, 1575-1582.
- 23 M. Fujishima, K. Tanaka, N. Sakami, M. Wada, K. Morii, T. Hattori, Y. Sumida and H. Tada, *J. Phys. Chem. C*, 2014, **118**, 8917-8924.
- 24 N.-G. Park, J. van de Lagemaat and A. J. Frank, *J. Phys. Chem. B*, 2000, **104**, 8989-8994.
- 25 T. Toyoda, T. Uehata, R. Suganuma, S. Tamura, A. Sato, K. Yamamoto, Q. Shen and N. Kobayashi, *Jpn. J. Appl. Phys.*, 2007, **46**, 4616-4621.
- 26 T. Toyoda, W. Yindeesuk, K. Kamiyama, S. Hayase and Q. Shen, *J. Phys. Chem. C*, 2014, **118**, 16680-16687.
- 27 P. Sudhagar, T. Song, D.-H. Lee, I. Mora-Seró, J. Bisquert, M. Laudenslager, W. M. Sigmund, W.-H. Park, U. Paik and Y.-S. Kang, *J. Phys. Chem. Lett.*, 2011, **2**, 1984-1990.
- 28 J. Xu, X. Yang, H. Wang, X. Chen, C. Luan, Z. Xu, Z. Lu, V. A. Roy, W. Zhang and C.-S. Lee, *Nano Lett.*, 2011, **11**, 4138-4143.
- 29 A. S. Nair, R. Jose, Y. Shengyuan and S. Ramakrishna, *J. Colloid. Interf. Sci.*, 2011, **353**, 39-45.
- 30 O. K. Varghse, M. Paulose and C. A. Grimes, *Nanotechnol.*, 2009, **4**, 592-597.
- 31 W. Shockley and H. J. Queisser, *J. Appl. Phys.*, 1961, **32**, 510-519.
- 32 J. E. G. J. Wijnhoven and W. L. Vos, *Science*, 1998, **281**, 802-804.
- 33 P. Lodahl, A. Floris van Driel, I. S. Nikolaev, A. Irman, K. Overgaag, D. Vanmaekelbergh and W. L. Vos, *Nature*, 2004, **430**, 654-657.
- 34 E. Yablonovitch, *Phys. Rev. Lett.*, 1987, **58**, 2059-2062.
- 35 K. Sakoda, M. Sasada, T. Fukushima, A. Yamanaka, N. Kawai and K. Inoue, *J. Opt. Soc. Am. B*, 1999, **16**, 361-365.
- 36 Z.-Z. Gu, S. Kubo, W. Qian, Y. Einaga, D. A. Tryk, A. Fujishima and O. Sato, *Langmuir*, 2001, **17**, 6751-6753.
- 37 D. Wang, A. L. Rogach and F. Caruso, *Chem. Mater.*, 2003, **15**, 2724-2729.
- 38 S. Nishimura, N. Abrams, B. A. Lewis, L. I. Halaoui, T. E. Mallouk, K. D. Benkstein, J. van de Lagemaat and A. J. Frank, *J. Am. Chem. Soc.*, 2003, **125**, 6306-6310.
- 39 L. I. Halaoui, N. M. Abram and T. E. Mallouk, *J. Phys. Chem. B*, 2005, **109**, 6334-6442.
- 40 L. J. Diguna, M. Murakami, A. Sato, Y. Kumagai, T. Ishihara, N. Kobayashi, Q. Shen and T. Toyoda, *Jpn. J. Appl. Phys.*, 2006, **45**, 5563-5568.
- 41 M. El Harakeh and L. I. Halaoui, *J. Phys. Chem. C*, 2010, **114**, 2806-2813.
- 42 J.-H. Shin and J.-H. Moon, *Langmuir*, 2011, **27**, 6311-6315.
- 43 Y.-G. Seo, K. Woo, J. Kim, H. Lee and W. Lee, *Adv. Funct. Mater.*, 2011, **21**, 3094-3103.
- 44 M. Samadpour, S. Giménez, P. P. Boix, Q. Shen, M. E. Calvo, N. Taghavunia, A. Irajizad, T. Toyoda, H. Míguez and I. Mora-Seró, *Electrochim. Acta*, 2012, **75**, 139-147.
- 45 H.-N. Kim and J.-H. Moon, *Curr. Appl. Phys.*, 2013, **13**, 841-845.
- 46 S. Meng, D. Li, X. Zheng, J. Wang, J. Chen, J. Fang, Y. Shao and X. Fu, *J. Mater. Chem. A*, 2013, **1**, 2744-2747.
- 47 S. Lee, Y. Lee, D.-H. Kim and J.-H. Moon, *ACS Appl. Mater. Interfaces*, 2013, **5**, 12526-12532.
- 48 X. Zheng, S. Meng, J. Chen, J. Wang, J. Xian, Y. Shao, X. Fu and D. Li, *J. Phys. Chem. C*, 2013, **117**, 21263-21273.
- 49 A. Rosencwaig and A. Gersho, *J. Appl. Phys.*, 1976, **47**, 64-69.
- 50 Y. Inoue, T. Toyoda and J. Morimoto, *Jpn. J. Appl. Phys.*, 2006, **46**, 4604-4608.
- 51 T. Toyoda, S. Tsugawa and Q. Shen, *J. Appl. Phys.*, 2009, **105**, 034314.
- 52 T. Toyoda, K. Oshikane, D. Li, Y. Luo, Q. Meng and Q. Shen, *J. Appl. Phys.*, 2010, **108**, 114302.
- 53 H. Yoo, M. Kim, C. Bae, S. Lee, H. Kim, T. K. Ahn and H. Shen, *J. Phys. Chem. C*, 2014, **118**, 9726-9732.
- 54 J. Marzin, J. Gérard, A. Izraël, D. Barrier and G. Bastard, *Phys. Rev. Lett.*, 1994, **73**, 716-719.
- 55 N. Greenham, X. Peng and A. Alivisatos, *Phys. Rev. B*, 1996, **54**, 17628-17637.
- 56 M. Honda, K. Kanai, K. Komatsu, Y. Ouchi, H. Ishii and K. Seki, *J. Appl. Phys.*, 2007, **102**, 103704.
- 57 Y. Nakayama, S. Machida, T. Minari, K. Tsukagishi, Y. Noguchi and H. Ishii, *Appl. Phys. Lett.*, 2008, **93**, 173305.
- 58 K. Kawabata, Y. Nanai, S. Kimura and T. Okuno, *Appl. Phys. A*, 2012, **107**, 213-220.
- 59 J. M. Ballantyne, *Phys. Rev. B*, 1972, **6**, 1436-1455.
- 60 A. Rosencwaig, *Anal. Chem.*, 1975, **47**, 592A-604A.
- 61 F. Urbach, *Phys. Rev.*, 1953, **92**, 1324.
- 62 N. Daude, C. Gout and C. Jouanin, *Phys. Rev. B*, 1977, **15**, 3229-3235.
- 63 N. Serpone, D. Lawless and R. Khairutdinov, *J. Phys. Chem.*, 1995, **99**, 16646-16654.
- 64 N. D. Abazović, M. I. Čomor, M. D. Dramićanin, D. J. Jovanović, S. P. Ahrenkiel and J. M. Nededjković, *J. Phys. Chem. B*, 2006, **110**, 25366-25370.
- 65 W. C. Dash and R. Newman, *Phys. Rev.*, 1955, **99**, 1151-1155.
- 66 X. Zhang, Y. Liu, S.-T. Lee, S. Yang and Z. Kang, *Energy Environ. Sci.*, 2014, **7**, 1409-1419.
- 67 G. D. Cody, T. Tiedje, B. Abeles and Y. Goldstein, *Phys. Rev. Lett.*, 1981, **47**, 1480-1483.
- 68 A. Meeder, D. Fuertes Marrón, A. Rumberg and M. Ch. Lux-Steiner, *J. Appl. Phys.*, 2002, **92**, 3016-3020.
- 69 D. A. Drabold, Y. Li, B. Cal and M. Zhang, *Phys. Rev. B*, 2011, **83**, 045201.
- 70 D. A. Jones and J. U. Lee, *Nano Lett.*, 2011, **11**, 4176-4179.
- 71 S. De Wolf, J. Holovsky, S.-J. Moon, P. Löper, B. Niesen, M. Ledinsky, F.-J. Haug, J.-H. Yum and C. Ballif, *J. Phys. Chem. Lett.*, 2014, **5**, 1035-1039.
- 72 A. Sadhanala, F. Deschler, T. H. Thomas, S. E. Dutton, K. C. Goedel, F. C. Hanusch, M. L. Lai, U. Steiner, T. Bein, P. Docampo, D. Cahen and R. H. Friend, *J. Phys. Chem. Lett.*, 2014, **5**, 2501-2505.
- 73 H. Sumi and Y. Toyozawa, *J. Phys. Soc. Jpn.*, 1971, **31**, 342-358.
- 74 M. Schreiber and Y. Toyozawa, *J. Phys. Soc. Jpn.*, 1982, **51**, 1528-1536.
- 75 H. Tang, F. Lévy, H. Berger and P. E. Schmid, *Phys. Rev. B*,

- 1995, **52**, 7771-7774.
- 76 L. Cavigli, F. Bogani, A. Vinattieri, V. Faso and G. Baldy, *J. Appl. Phys.*, 2009, **106**, 053516.
- 77 Y. Yamada and Y. Kanemitsu, *Appl. Phys. Lett.*, 2012, **101**, 133907.
- 78 J. Preclíková, P. Galář, F. Trojánek, S. Daniš, B. Rezek, I. Gregora, Y. Němcová and P. Malý, *J. Appl. Phys.*, 2010, **108**, 113502.
- 79 Y. Lei, L. D. Zhang, G. W. Meng, G. H. Li, X. Y. Zhang, C. H. Liang, W. Chen and S. X. Wang, *Appl. Phys. Lett.*, 2001, **78**, 1125-1127.
- 80 B. Choudhury and A. Choudhury, *Physica E*, 2014, **56**, 364-371.
- 81 R. J. Elliot, *Phys. Rev.*, 1957, **108**, 1387-1389.
- 82 B. Enright and D. Fitzmaurice, *J. Phys. Chem.*, 1996, **100**, 1027-1035.
- 83 A. Stashans, S. Lunell and R. W. Grimes, *J. Phys. Chem. Solids*, 1996, **57**, 1293-1301.
- 84 J. Chen, L.-B. Lin and F.-Q. Jing, *J. Phys. Chem. Solids*, 2001, **62**, 1257-1262.
- 85 H. Zhang, M. Zhou, Q. Fu, B. Lei, W. Lin, H. Guo, M. Wu and Y. Lei, *Nanotechnology*, 2014, **25**, 275603.
- 86 M. M. Maitani, K. Tanaka, D. Mochizuki and Y. Wada, *J. Phys. Chem. Lett.*, 2011, **2**, 2655-2659.
- 87 Y. Zhou, C. Fuentes-Hernandez, J. Shim, J. Meyer, A. J. Giordano, H. Li, P. Winger, T. Papadopoulos, H. Cheun, J. Kim, M. Fenoll, A. Dindar, W. Haske, E. Najafabadi, T. M. Khan, H. Sojoudi, S. Barlow, S. Graham, J.-L. Brédas, S. R. Marder, A. Kahn and B. Kippelen, *Science*, 2012, **336**, 327-332.
- 88 K. Nishimori, K. Tanaka and Y. Inoue, *J. Appl. Phys.*, 1991, **69**, 8042-8046.
- 89 T. Hanmin and L. Shoubin, *Adv. Biomed. Eng.*, 2012, **8**, 59-63.